# Dependence of Ductility Response Spectra on the Seismogenic Depth from Finite Element Earthquake Rupture Simulations

*Gangapoguu Venkata Kishor[1*] and Surendra Nadh Somala[2]*

1. M. Tech, Department of Civil Engineering, Indian Institute of Technology, Hyderabad, India,
* Corresponding Author; email: ce15mtech11018@iith.ac.in
2. Assistant Professor, Department of Civil Engineering, Indian Institute of Technology,
Hyderabad, India

## ABSTRACT

*Ongoing research in the development of design philosophies for earthquake resistant structures over the past few decades was initially based on the strength and elastic analysis. Later, design philosophies recognized the deformation to be an important parameter to be considered in design following nonlinear analysis. The maximum design lateral force, for a particular earthquake, acting on structures having multiple natural time periods can be obtained from inelastic response spectrum. Scenario earthquakes characterize the spatio-temporal evolution of fault rupture, which when solved together with the elastodynamic equations can give the acceleration time-history at any point on the surface. For any tectonic regime, based on the past seismicity, a seismogenic depth could be defined based on the depth below which no occurrence of earthquakes was observed in the past. Fixing a certain magnitude, we prescribe the slip on a vertical fault based on statistical relations that exist in literature, and simulate ground motion. The ruptured region is varied, is initially assumed to be closer to the free surface, and is later lowered deeper in intervals of 10 km to emulate larger seismogenic depths. Using the simulated ground motion, we compute the fundamental entity of earthquake engineering: the response spectrum for five depths of hypocenter. Earthquake resistant design of structures is mostly done to allow for large inelastic deformations, giving ductile detailing. Choosing ductility ratios of 2, 4, 6 and 8, this paper describes dependency of elastic and inelastic horizontal spectral acceleration on seismogenic depth, by considering kinematic rupture description of a Mw 6.5 earthquake on a vertical strike slip fault.*

## 1. Introduction

As earthquake is an unpreventable natural event, to decrease its effect on loss of lives and property, the proper understanding of source parameters, rake angle and ductile detailing of engineering structure is required. Source parameters give information related to the magnitude of slip over finite dimension and its temporal evolution. Strike slip, dip slip and oblique slip are three classifications based on rake angle. Source parameters are specific to an earthquake but the ductile detailing of structure in a specific region depends on the history of earthquakes and intended ductility in structure.

In the seismic analysis of structures like buildings, nuclear power plants, bridges etc. time history of ground motion at that specific location is necessary to compute the seismic demand. The necessity of synthetic ground motion comes where there is a lack of sufficient recording stations. Because of the

S- and P-wave radiation pattern, the ground motion can be azimuthally dependent and so sometimes a single-station near-source recording for an earthquake may not be sufficient for engineering analysis. In addition, a catalog of earthquake records is necessary for advanced research like performing seismic reliability assessment and for Incremental Dynamic Analysis (IDA). Due to these reasons, the generation of synthetic ground motion records got its importance in the field of seismic engineering.

Generally, methods of generating of synthetic ground motion records can be categorized as (a) simple scaling of actual ground motion records in time domain, (b) response spectral matching of existed records (c) convolving source time function (STF) with pre-computed Green's function. Among them, each method has its own limitations to use. Synthetic motions generated using simple scaling method will lack differences in important parameters like frequency and duration. Synthesis of ground motions using frequency domain method are not specific to an event but to target response spectra. Convolving Green's functions with unified source time function is debatable as there is possibility of variation in rupture duration over the fault plane. Nevertheless, Green's functions can account for important near-field effects like directivity. Weighted summation of Green's functions from each sub-faults, on a partitioned fault plane, to a given site can give the overall time-dependent response of the ground. Solvers for 3D wave equations for media with discontinuities can do this internally and give the time-histories of ground shaking all over the surface of the earth, that is part of the domain of consideration.

When a system is subjected to randomized cyclic loading like an earthquake, each system having different time period will behave differently. In the design of structures for cyclic loading, it is very important to calculate seismic demand on structure, which may be maximum induced lateral force (elastic) or reduced lateral force (inelastic) for corresponding ductility ratio. The lateral force is the product of seismic mass of system and PSA (pseudo spectral acceleration) at structure's natural frequency. PSA can be obtained by solving dynamic equilibrium equation for a particular natural frequency. The maxima of such PSA for various natural frequencies is the response spectrum.

In order to understand the variations in response spectrum (PSA values for selected time periods), we simulate ground motions for a specific magnitude strike-slip earthquake on a vertical fault plane. Finite fault dimensions of the chosen magnitude earthquake are obtained by scaling relations and rupture description of earthquake prescribed based on existing empirical relations. The simulated ground motion is used to compute elastic and inelastic spectral acceleration distribution. By varying the depth to the top of the fault, we study the variation in spectral acceleration.

Mavroeidis et al [1] developed an empirical mathematical model for near-field ground motions and compared elastic and inelastic response spectrum of SDOF system for both simulated and actual ground motion records. Empirical ground motion attenuation relationships were developed by Campbell et al [2], which were shown to be good at predicting spatial variability of PGA (peak ground acceleration), PGV (peak ground velocity), PGD (peak ground displacement) and elastic and inelastic response spectra. However, those are applicable for shallow continental earthquake occurs in locations, which have similar faults like Western North America. To the best of our knowledge, no author has addressed the variation in spectral acceleration as a function of depth of a kinematic rupture description for a given magnitude, particularly from simulated 3D ground motion perspective.

## 3. Methodology

To simulate synthetic ground velocities due to the prescribed earthquake rupture, we chose to use Pylith software developed by Aagaard et al [3]. Pylith is a C++ code with Python wrappers interfaced by SWIG to compute lithospheric deformation using finite element approach. It facilitates modeling of wave propagation due to the propagating kinematic ruptures on high-performance supercomputing facilities using Message Passing Interface (MPI).

The wave equation in differential form, obtained by applying Lagrangian description of momentum conservation over a volume $V$, bounded by surface $S$, is:

$$\rho \frac{\partial^2 u_i}{\partial t^2} - f_i - \sigma_{ij,j} = 0 \qquad (1)$$

where $\rho$ is a density, $u_i$ is displacement vector, $f_i$ is body force and $\sigma_{ij,j}$ is divergence of stress vector, i.e. it traction over fault surface.

The weighted residual method was used to convert strong form of the wave equation to weak form and continuous Galerkin method was implemented to solve integral equations. In Galerkin method, shape function and weighting functions are the same. Incorporating explicit Newmark time-stepping scheme, the weak form is solved using PETSc [4]. Fault discontinuity in Pylith is handled by insertion of cohesive element between the two sides of the fault and constraining the slip to be prescribed amount using Lagrange multipliers [3]. Pylith can simulate wave field in parallel across several processors using Message Passing Interface (MPI) after decomposing the domain and distributing it using ParMETIS.

## 4. Inputs

Pylith expects all the parameters that are essential for simulation in specific formats. First, a finite element mesh of the domain that surrounds the fault plane by a few tens of km on all sides is exported in Exodus format from CUBIT [5]. Second, spatial database files, simply ASCII files with metadata, provide spatial variation of parameters like slip, slip time, rise time, material properties. Third, configuration files that contain details about boundary conditions, linear/nonlinear solver, fault and formulation of the problem.

### 4.1. Meshed Geometry and Highest Frequency Resolved

A domain of dimensions 60×60×60 km is chosen with a vertical planar discontinuity in the middle of domain (fault plane) parallel to y-axis as shown in Figure (1a). Only a portion of this pre-existing discontinuity ruptures during an earthquake. Choice
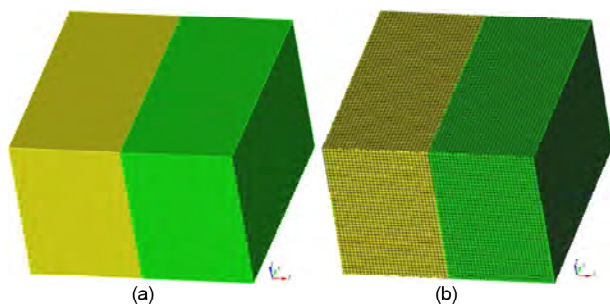


**Figure 1.** (a) Domain geometry with fault plane (b) sample mesh.

of the domain size is based on region of influence within which the ground shaking is reduced by approximately an order of magnitude compared to the epicentral shaking, as we approach the boundaries of the domain. The domain is meshed with hexahedral elements using CUBIT software (Figure 1b). Layered isotropic, elastic material is considered with one-dimensional velocity model. For preliminary case of simulation where we studied statistically dependency of simulated parameters on rupture description, hexahedral elements of size 1 km is used. With this mesh size, the minimum time period of 1.25 sec [6] can be achieved, which falls slightly outside the range where civil engineering structures fall. To push towards lower time periods where many of the low-rise buildings belong to, we have also attempted a 200 m mesh, which can simulate the ground motion accurately up to the minimum time period of 0.25 sec [6]. Note that a reduction in mesh size by half increases the computation requirement by a factor of 16, as the number of elements gets doubled along all three dimensions and stable time step reduces by a factor of 2.

### 4.2. Rupture Description

Kinematic rupture modeling requires the distribution of slip, rupture time and rise time over the ruptured area. For lack of sufficient statistics on distribution of rise time in literature, it is assumed to be constant over the entire rupture area and is fixed as 1 sec [7]. The variation of slip and slip time on ruptured area are shown in Figure (2). Rupture dimensions are computed using Mai and Beroza [8] empirical equations. Mai and Beroza [9] have developed stochastic characterization of slip, which suggests that slip distribution can be modeled as an anisotropic von Karman random field. Correlation lengths or spectral decay parameters in dip direction, strike direction and Hurst number that characterize the von Karman autocorrelation function are computed based on length and width of fault, according to the historic strike-slip ruptures [9]. Hypocentre location is assumed as location where max slip has occurred over ruptured area. As the slip distribution is random, hypocentre location is also in random nature. Rupture velocity is taken as 0.8 times the shear wave velocity [10]. Additionally, random

perturbation in rupture velocity is also introduced to account for heterogeneity. All the source parameters which are used to define rupture description are shown in Table (1). Liu-cosine slip-time function [11] slip time function is considered to model temporal evolution. It creates finite duration of slip with intense rise and slow termination with time.

In this work, denoting the minimum depth to top of the rupture from the surface by $h_{top}$, we chose five different $h_{top}$s (3 km, 13 km, 23 km, 33 km and 43 km) for prescribing the rupture on the fault plane. In the preliminary case of simulation, with mesh size of 1 km, 30 samples of rupture are chosen based on Latin hypercube sampling [12]. In the latter case of simulation, with mesh size of 200 m, only one rupture has been considered and is shown in Figure (2). For the samples generated with 1 km mesh, histograms of parameters like
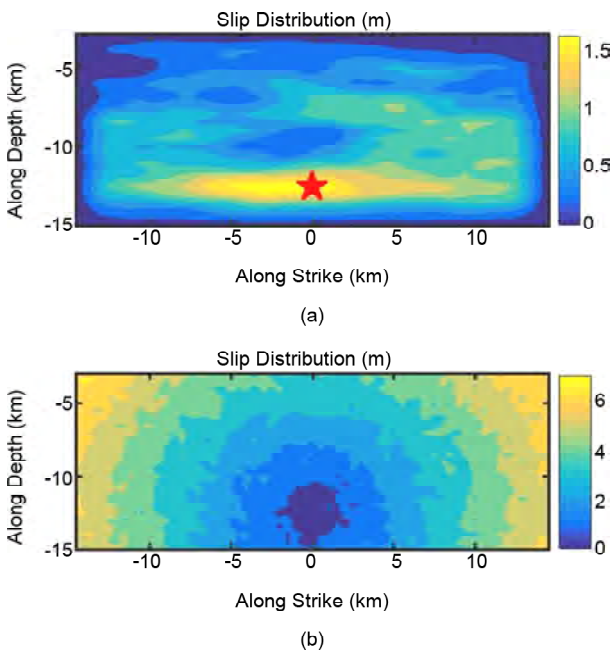


(a)



(b)

**Figure 2.** (a) Slip distribution (b) slip time distribution over the ruptured area for case of htop is 3 km.

**Table 1.** List of seismic parameters considered in computing slip, slip time distribution.

| Name of Source Parameter | Value Considered |
|---|---|
| Magnitude, Mw | 6.5 |
| Hypocenter | Sub-Fault with Maximum Slip |
| Source Mechanism | Strike Slip |
| Strike | $0^0$ |
| Dip | $90^0$ |
| Rake | $180^0$ |
| Ratio of Rupture Wave to Shear Wave Velocity | 0.8 + Random Perturbation |

hypocentral depth, epicenter location are shown in Figure (3) and the histograms of rupture dimensions are shown in Figure (4).
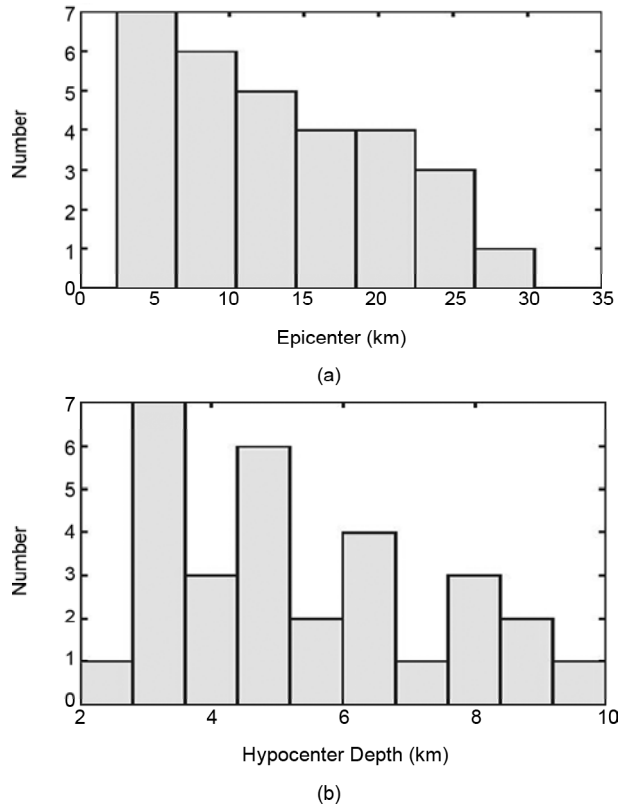


(a)



(b)

**Figure 3.** Distribution of (a) Epicenter (b) Hypocenter when htop is zero.
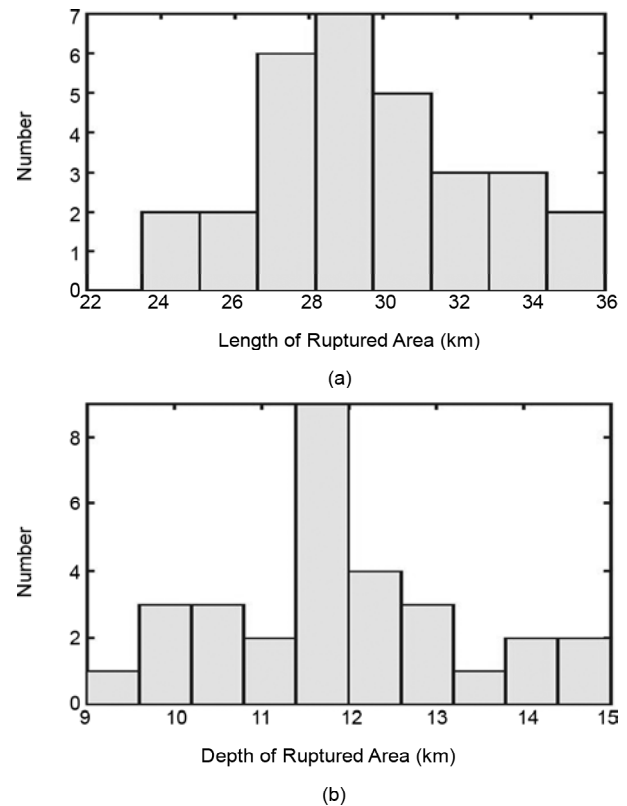


(a)



(b)

**Figure 4.** Distribution of (a) rupture length (b) rupture depth.

**Table 2.** Velocity model at source region.

| Depth (km) | Vp (km/s) | Vs (km/s) | Density (kg/m$^3$) |
|---|---|---|---|
| 0 - 1.9 | 5.54 | 3.2 | 2400 |
| 2.0 - 16.4 | 5.78 | 3.47 | 2610 |
| 16.5 -39.4 | 6.56 | 3.61 | 2700 |
| 39.5-53.5 | 7.41 | 4.28 | 3200 |
| >53.5 | 7.63 | 4.41 | 3300 |

### 4.3. Material Properties

Homogeneous, Isotropic elastic material is considered with one-dimensional layered velocity model (Table 2) was used for the domain based on Acton et al. [13] for Sikkim region that contains certain active right lateral strike slip faults [14]. It is noteworthy that the devastating earthquake in Sikkim on the evening of 18$^{th}$ September 2011, has strike slip source mechanism with a dip angle close to 90°. Absorbing boundary conditions have been considered on all faces of domain except ground surface to get rid of reflection of seismic waves.

### 5. Receiver Geometry for Statistical Analysis and Comparison of Spectra

Certain monitoring points (hereafter referred to as stations) are chosen to identify the distribution of spectral acceleration for a logarithmically spaced chosen set of time periods. One such array of stations is chosen in a radial grid fashion around origin at distances of 1 km, 5 km, 10 km, 15 km, 20 km, 25 km and 30 km as shown in Figure (5a). In total, these are 56 stations. At these stations, statistical analysis is performed. Finally, for the higher resolution mesh (mesh size smaller by a factor of 5) of 200 m, a near circular array of stations is chosen at a radius of 7 km around origin, and at angular spacing of 22.5° as shown in Figure (5b). In total, these are 16 stations. At these stations, response spectra are computed for elastic case (μ=1) and inelastic cases (μ=2, 4, 6, 8).

### 6. Results

The distribution of hypocentral depth, epicentral distance in Figure (3) appears to follow the beta distribution, while those of length and width of ruptured area in Figure (4) seem to follow the normal distribution. The distribution of hypocentral depth shown in Figure (3b), are for the case when



(a)



(b)
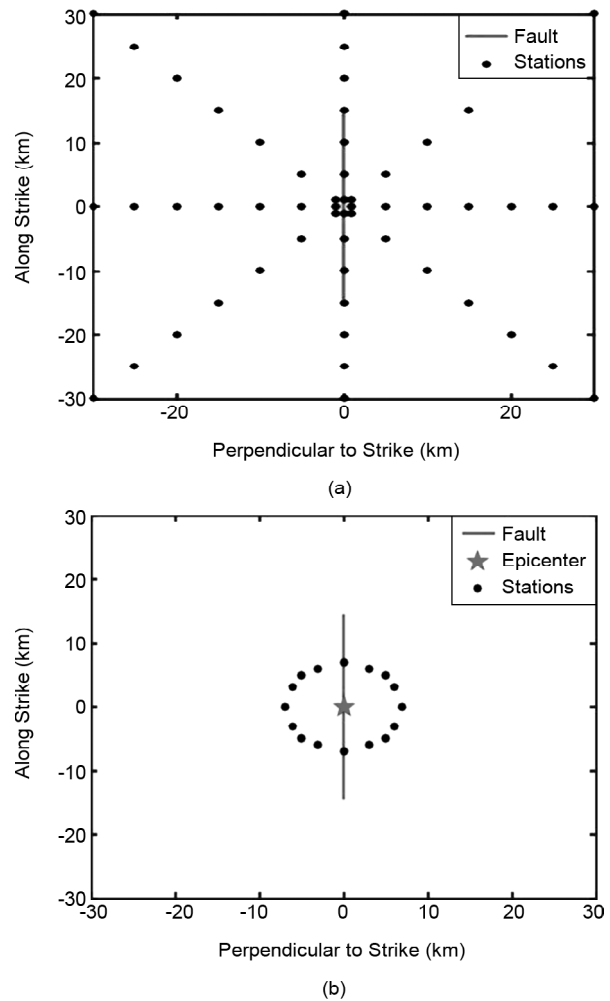
**Figure 5.** Stations considered in (a) grid fashion (b) circular fashion over surface with fault trace.

rupture reaches the surface. For any other $h_{top}$, hypocentral depth distribution needs to be shifted by as many units as $h_{top}$.

By considering the variability in hypocenter, epicenter and rupture dimensions, 30 simulations are performed on a domain shown in Figure (1a) with a mesh size of 1 km. We ran the kinematic rupture simulations in Pylith with parameters described in section 4, and computed the ground motion all over the top surface of the domain. Maxima of ground acceleration and ground displacements are computed for all the 30 samples at the free surface and contours of PGA, PGV and PGD in map view are shown in Figure (6) for a case of $h_{top}$ 3km. Fault parallel component of the acceleration is symmetric about axis perpendicular to fault, and a fault-normal component of acceleration is symmetric about axis parallel to fault. Along the nodal plane, fault parallel and vertical components of acceleration are almost zero while fault normal

component of acceleration has non-zero magnitude. The Euclidean norm of peak ground parameters show bi-lobed pattern symmetric with respect to the fault plane, with maxima away from the surface trace of the fault. Chi square test is performed on certain randomly picked station locations in Figure (5) and the Quantile-Quantile plots for PGA and PGD are shown in Figure (7). The red line in Figure (7) corresponds to Gaussian distribution. It can be seen that the distribution of PGA and PGD at all the stations nearly follows Gaussian distribution. Maximum standard deviation of PGA at all stations considered is 0.23g and the minimum is 0.01g. PGD was observed to follow trend similar to PGA, with minimum and maximum standard deviation values are 0.004 m, 0.071 m. Mean and standard deviation of PGA and PGD are tabulated in Table (3).

The joint probability mass functions (PMF) of spectral acceleration and time period are shown in
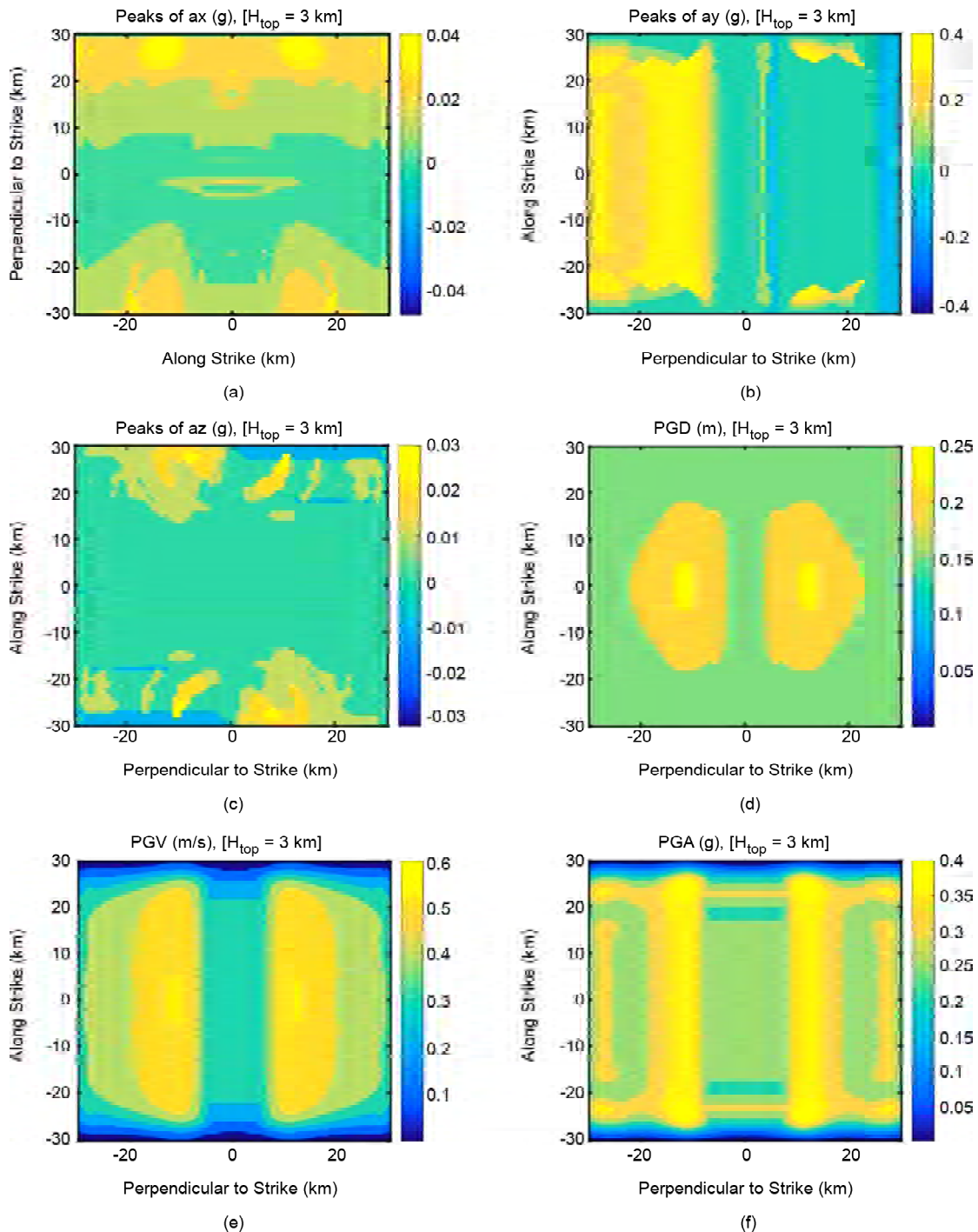
**Figure 6.** Plot showing contour maps of peak values of x, y, z components of acceleration (a, b, c) and norm of peak ground acceleration, peak ground velocity, peak ground displacement (d, e, f) while fault is in x = 0 plane.

Figure (8), at four stations of Table (3), which had higher PGA variance. It can be observed from this figure that as we approach time periods closer to 4 sec, there is high probability (near unity) that the spectral acceleration approaches the lowest bin considered. Intermediate time periods ranging somewhere between 0.37 sec to 0.82 sec have the highest spectral acceleration values. Moreover, the distribution of spectral acceleration appears to be log normal.

By comparing Figures (6a-c), the fault-parallel component has high magnitude. Therefore, Elastic Response Spectrum (ERS) and Inelastic Response Spectrum (IRS) contours with five different ductility ratios ($\mu$ = 1, 2, 4, 6, 8) at 16 stations shown in Figure (9) for a fault-parallel component of
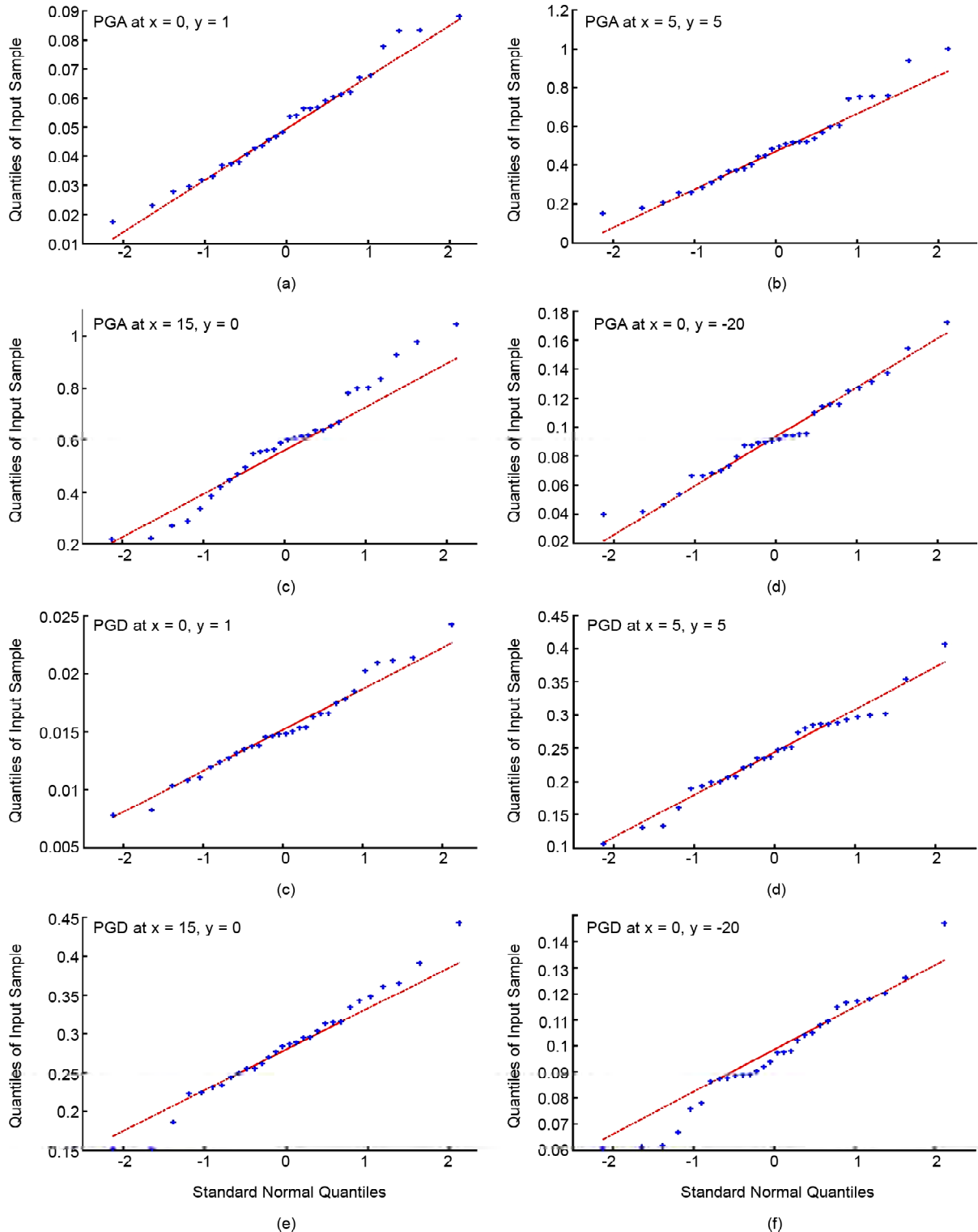
**Figure 7.** Quantile-Quantile plots for PGA, PGD shown a few selected stations from star grid geometry shown in Figure (5a).

**Table 3.** Distribution parameters for PGA, PGD at stations selected in grid fashion.

| Station No. | x-coord (km) | y-coord (km) | PGA (in g) | | PGD (in m) | |
|---|---|---|---|---|---|---|
| | | | Mean | Standard Deviation | Mean | Standard Deviation |
| 1 | -1 | 1 | 0.21 | 0.09 | 0.07 | 0.021 |
| 2 | 0 | 1 | 0.05 | 0.02 | 0.02 | 0.004 |
| 3 | 1 | 1 | 0.21 | 0.09 | 0.07 | 0.021 |
| 4 | 1 | 0 | 0.21 | 0.09 | 0.07 | 0.021 |
| 5 | 1 | -1 | 0.21 | 0.09 | 0.07 | 0.021 |
| 6 | 0 | -1 | 0.05 | 0.02 | 0.02 | 0.004 |
| 7 | -1 | -1 | 0.21 | 0.09 | 0.07 | 0.021 |
| 8 | -1 | 0 | 0.21 | 0.09 | 0.07 | 0.021 |
| 9 | -5 | 5 | 0.49 | 0.21 | 0.24 | 0.065 |
| 10 | 0 | 5 | 0.05 | 0.01 | 0.04 | 0.007 |
| 11 | 5 | 5 | 0.49 | 0.21 | 0.24 | 0.065 |
| 12 | 5 | 0 | 0.49 | 0.21 | 0.24 | 0.065 |
| 13 | 5 | -5 | 0.49 | 0.21 | 0.24 | 0.065 |
| 14 | 0 | -5 | 0.05 | 0.01 | 0.04 | 0.007 |
| 15 | -5 | -5 | 0.49 | 0.21 | 0.24 | 0.065 |
| 16 | -5 | 0 | 0.49 | 0.21 | 0.24 | 0.065 |
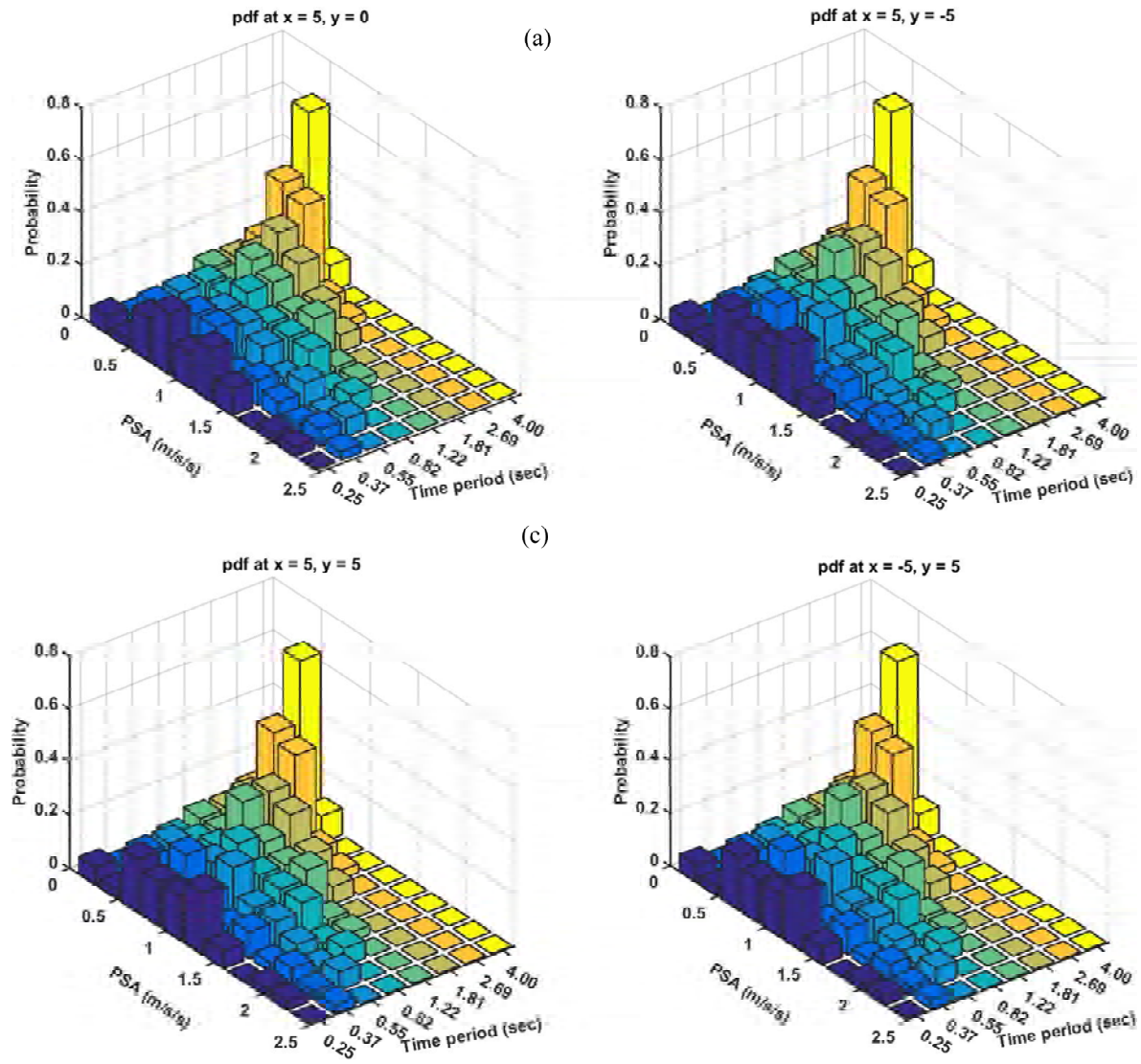


**Figure 8.** Probability Density Function for elastic PSA at different time periods for $h_{top}$ 3 km.
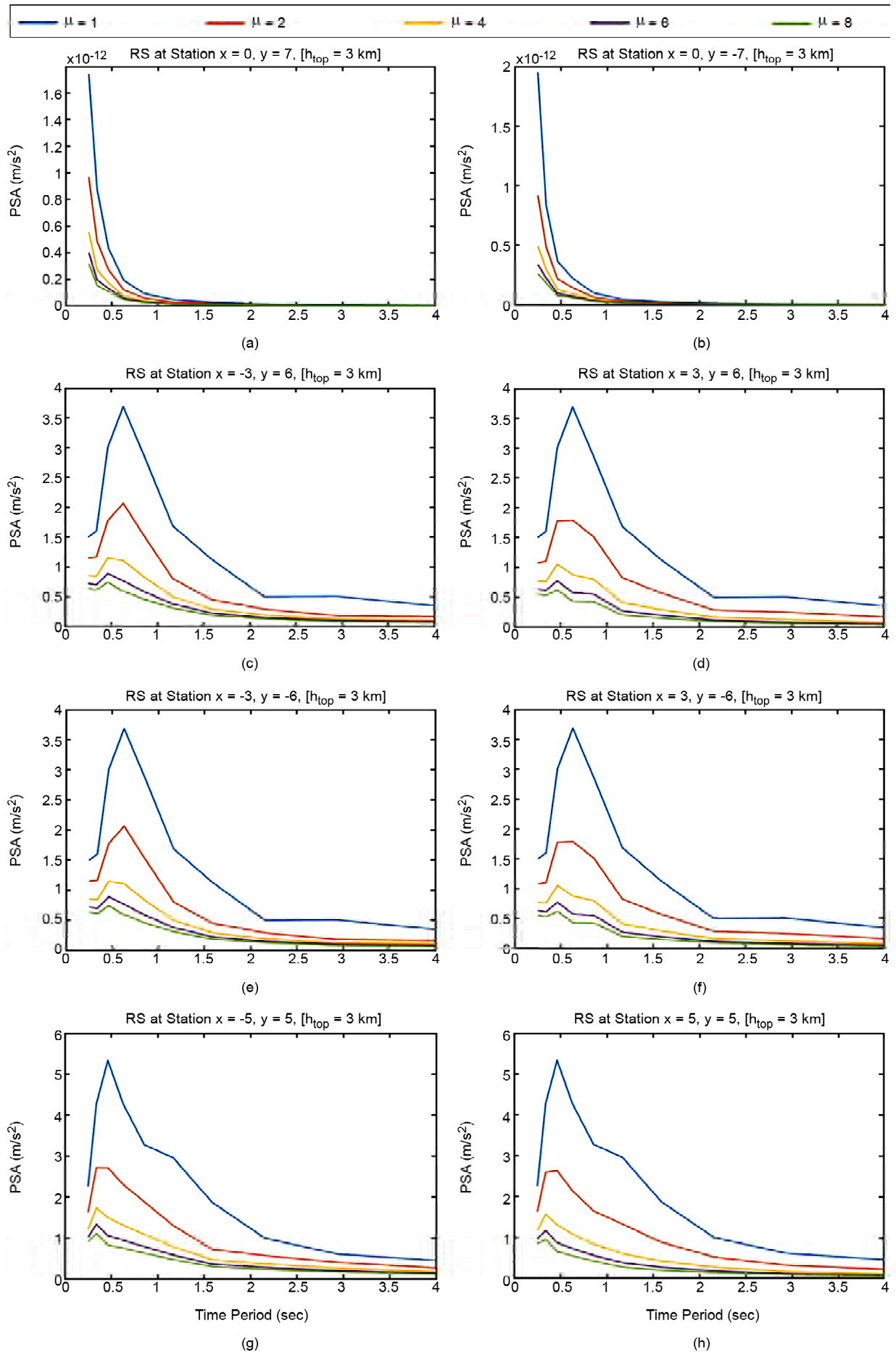
**Figure 9.** Plot showing response spectrum with different ductility ratios at 16 station.
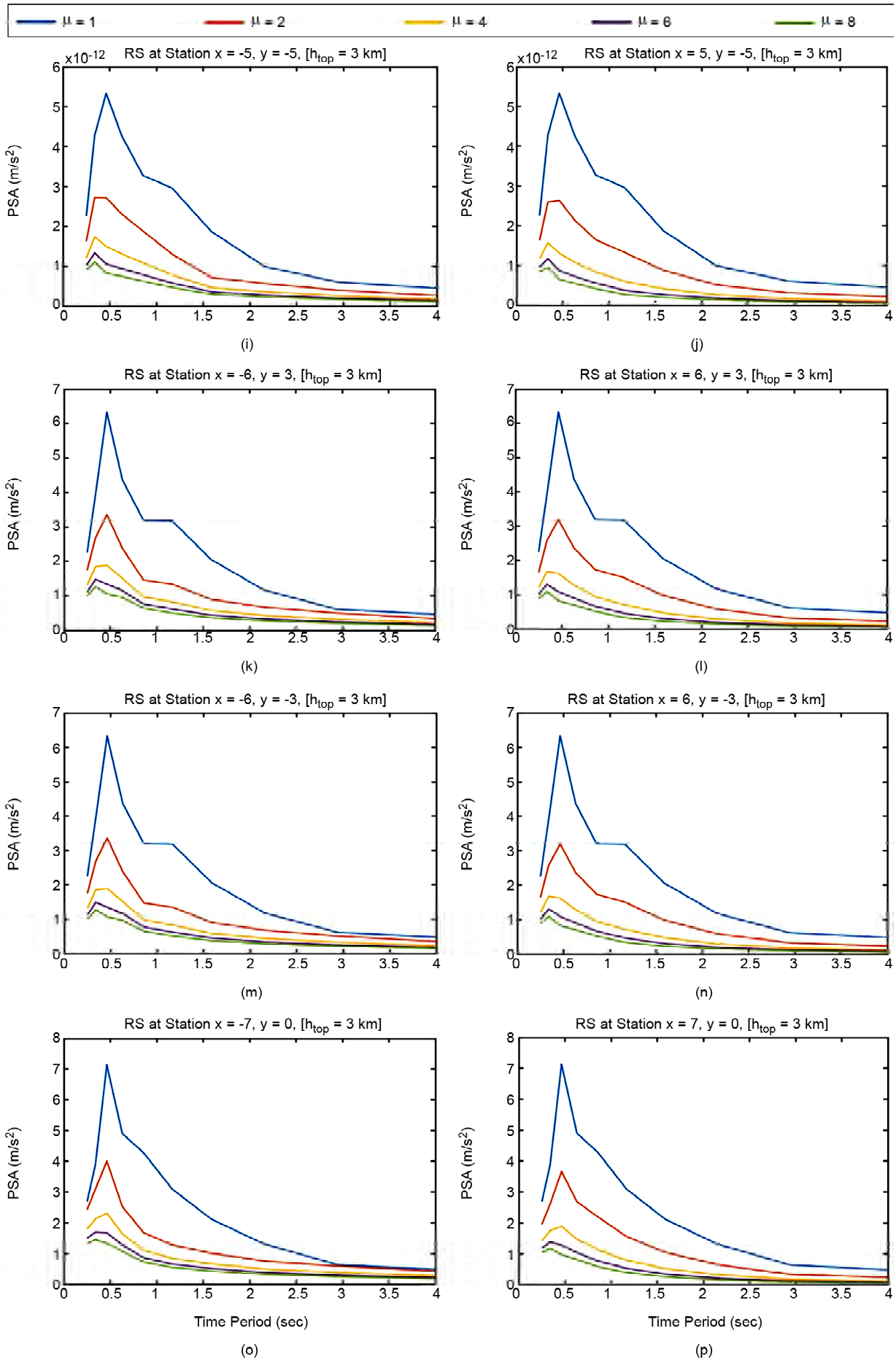
**Figure 9.** Continue.

acceleration by assuming material is elastic-perfectly plastic with a damping ratio of 5%. The symmetry of chosen station configuration (Figure 5b) with respect to both x, y-axes resulted in the same symmetry of y-component of acceleration records, which translated into symmetry of response spectrum about both x, y-axes. This is a clear evidence of radiation pattern. The directivity of rupture from negative y-direction to positive has resulted in asymmetry of ground motion at stations along strike on either side of the fault. Evidently, as the ductility ratio is increasing spectral values are decreasing, as expected, and thus the demand on structure. For the fault-parallel component of the acceleration, contours of spectral acceleration over the entire top surface are also computed for different time periods at all ductility ratios and for all $h_{top}$ cases. Figure (10) shows one such case, for $h_{top} = 3$ km, time period = 0.46 sec, con-sidering all ductility ratios. Clearly, the spectral acceleration was decreasing according to the ductility ratio, while maintaining the spatial variation in map view.

Contours of spectral acceleration for ductility ratio of 2 at different time period are shown in Figure (11), for $h_{top}$ 13 km case. As the civil engineering structures are mostly located in the acceleration sensitive region where spectral acceleration values increase with time period, it is better to know beforehand the time periods at which PSA values are high. This information helps an engineer
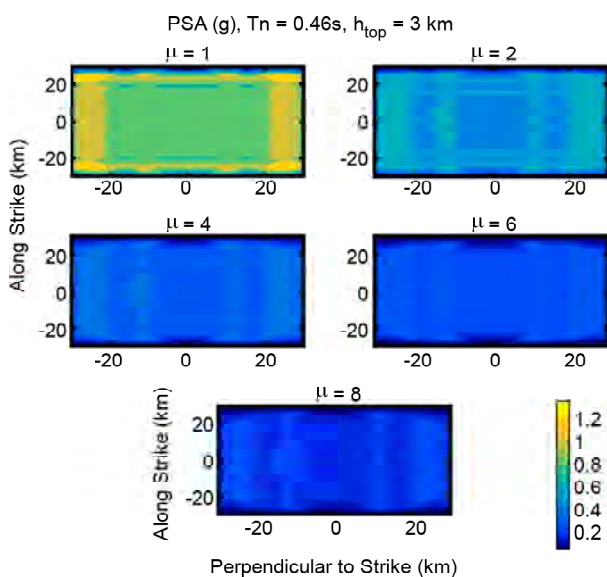
to ensure that the fundamental period of the structure does not fall close to such time periods of highest PSA, while designing the elements of a structure. Time period 0.63 sec shows highest PSA among the periods considered in this study. Structures having natural frequency close to this time period will undergo the resonance and have higher failure probability, for this particular scenario.

Furthermore, variation in elastic response spectrum as a function of $h_{top}$ (3 km, 13 km, 23 km, 33 km, 43 km) is shown in Figure (12). Understandably, embedding the rupture deeper and deeper, for a given magnitude earthquake lowers the spectral acceleration, but this figure also conveys the amount by which the spectral acceleration gets reduced. At time period of 0.46 sec, contours of elastic PSA for various cases of $h_{top}$ are shown in Figure (13). A drastic reduction in PSA by roughly a factor of 5 is observed, up on lowering the fault rupture from 3 km to 13 km. However, the ratio of reduction in PSA is lower for further 10 km deeper fault ruptures.

The variations of PGA and PSA for ductility ratio 2 at time period of 0.46 sec over ground surface are shown in Figure (14). Spatial pattern of PSA almost corresponds to that of PGA for this case. With an increase in $h_{top}$ by lowering the hypocenter, the maximum PGA over the top surface of the domain is found to be decreasing and the areas that will be affected most by earthquake are located farther away from the nodal plane. The ratio between maximum values of PSA and PGA is in between 1.4 to 1.56 for this particular period and ductility ratio.

Given the symmetric nature of fault-parallel component of PGA and PSA, here, we only consider the stations from the first quadrant of Figure (5a) to quantify the reduction in PSA with depth of hypocenter. In Figure (15), percentage reduction in elastic PSA is represented as bar graph. The trend in PSA obviously depends on the ground motion at that station, which in turn depends on the medium between the station and the hypocenter. When $h_{top}$ is varied lowered till 33 km, from 3 km, almost at all stations show monotonically decreasing trend (Figure 15) of elastic PSA at all time periods considered (0.25 sec to 4 sec) in this study. For the case of $h_{top}$ 43 km (i.e. hypocenter is located at 52.5 km
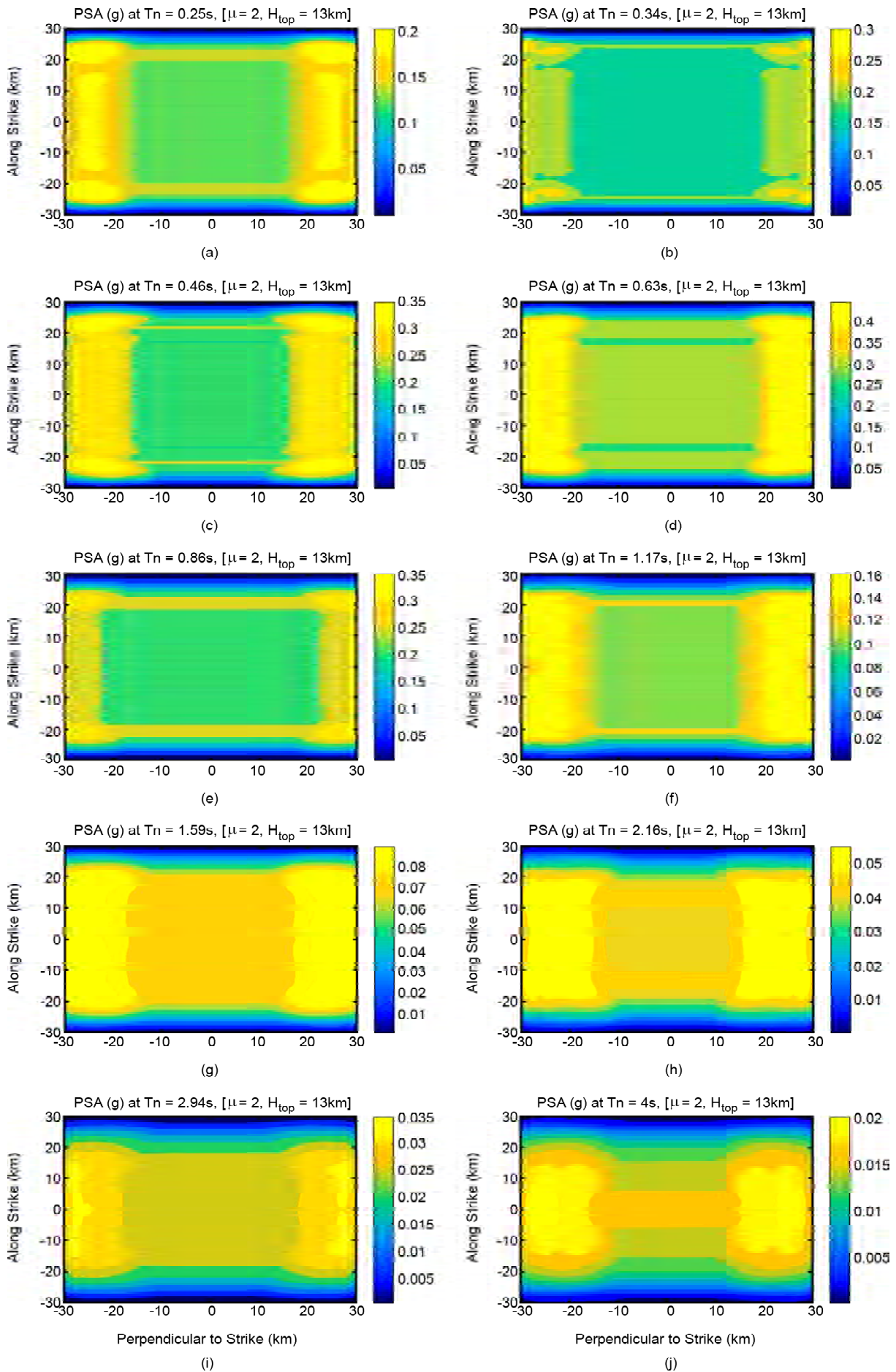


**Figure 10.** Plots showing contours of PSA due to the fault parallel component of acceleration over surface at time period 0.46 sec with ductility ratio 1, 2, 4, 6, 8 for case of $h_{top}$ 3 km.

**Figure 11.** Contours of inelastic PSA with ductility ratio 2 at different time periods, for case of h_top 13 km.

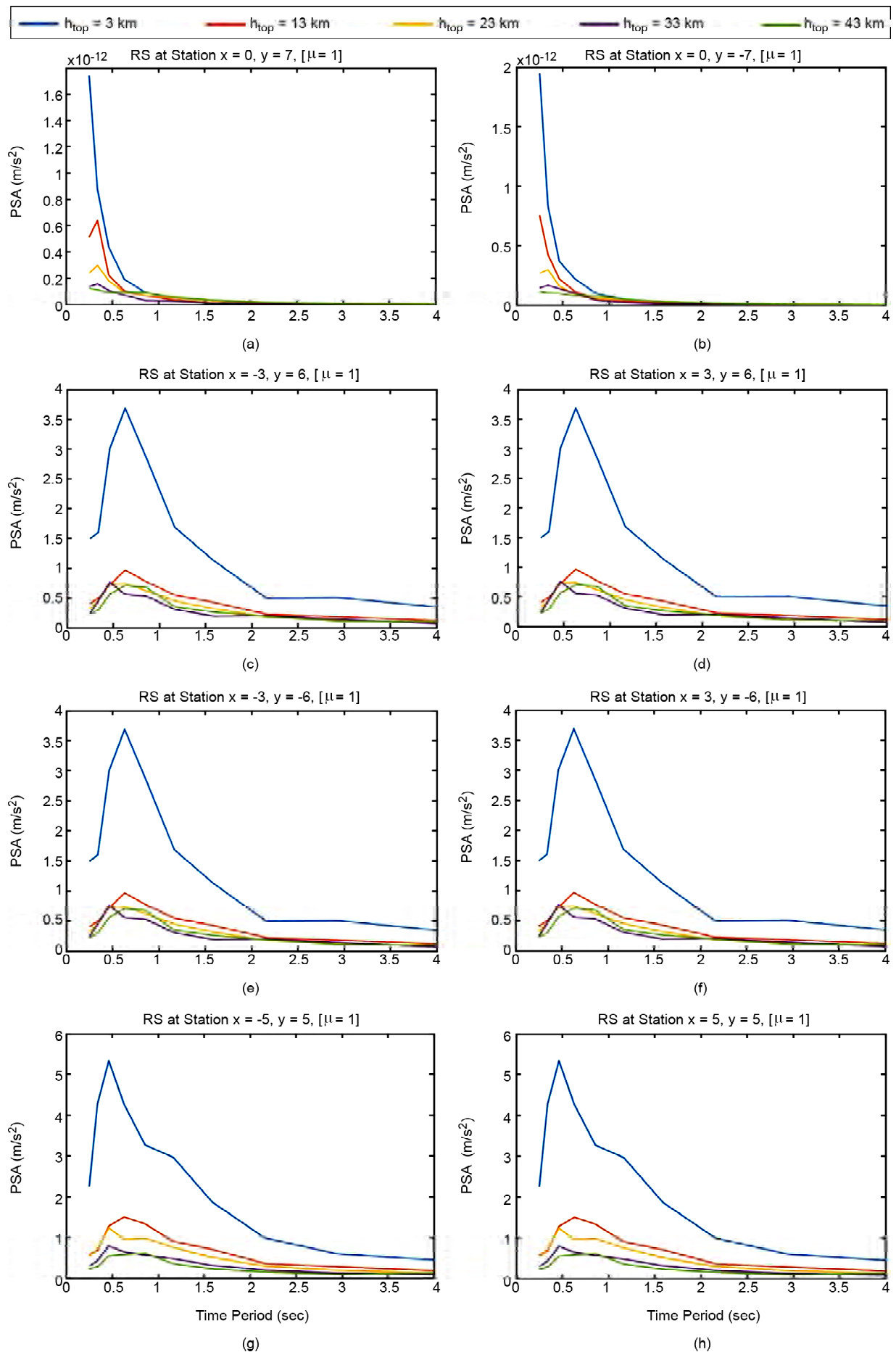**Figure 12.** Plots showing elastic response spectrum at 16 stations for $h_{top}$ = 2, 4, 6, 8, 10 km.
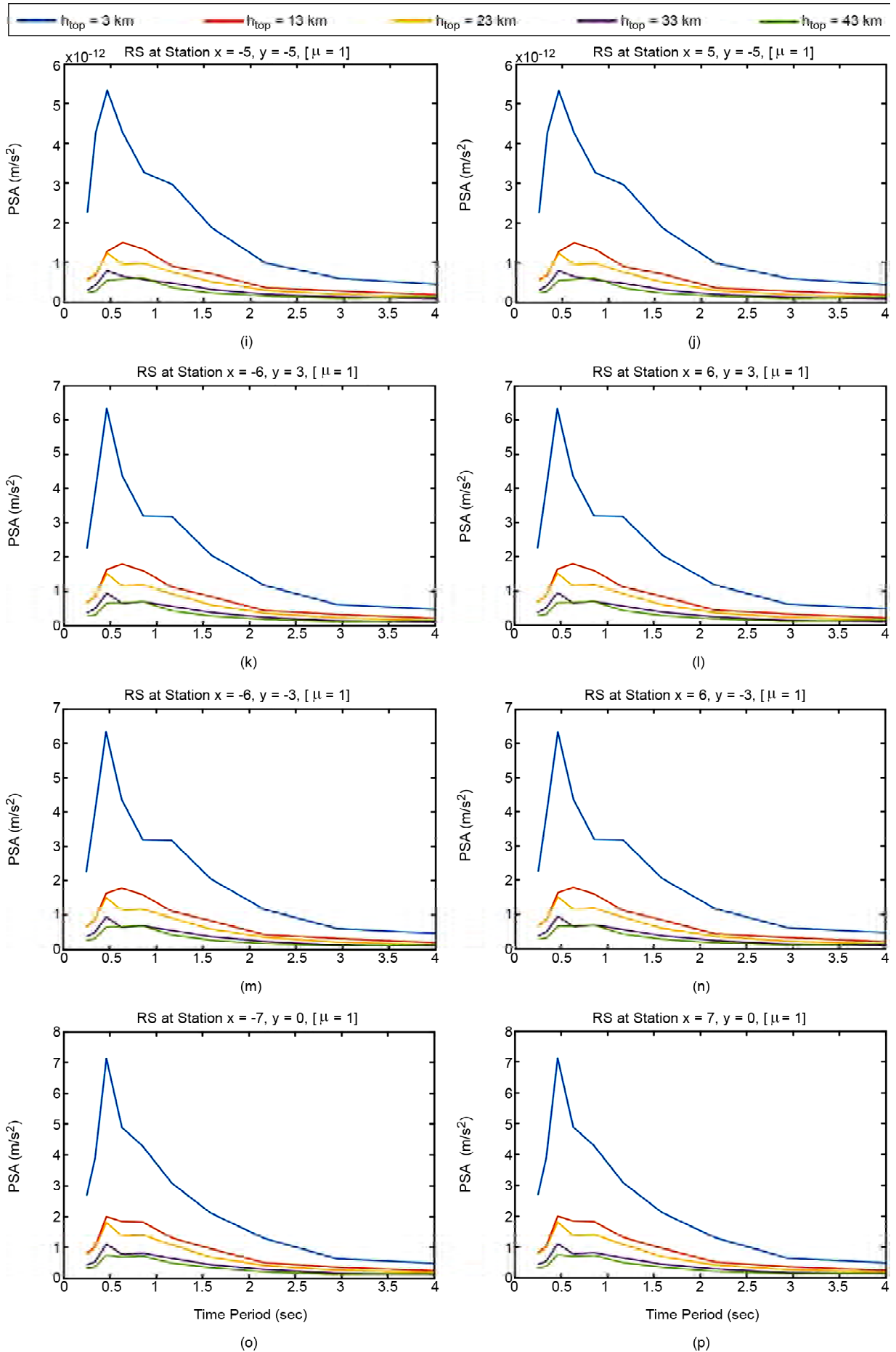
**Figure 12.** Continue.

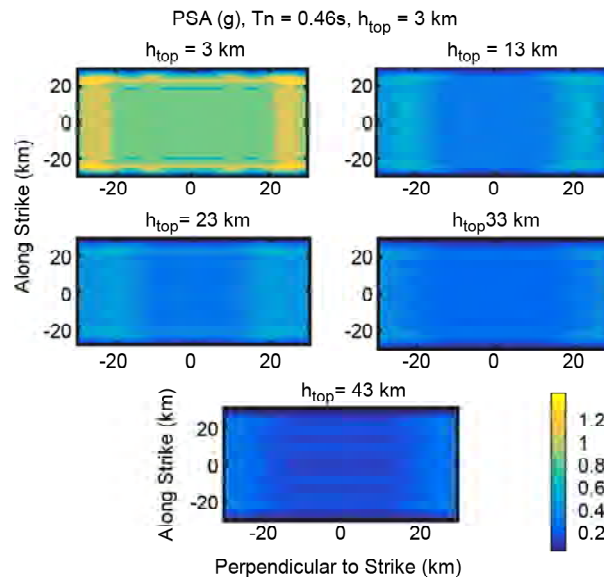PSA (g), Tn = 0.46s, h$_{top}$ = 3 km



**Figure 13.** Variation of elastic PSA (g) at time period of 0.46 sec with h$_{top}$.

**Table 4.** Maximum and minimum percentage reduction in PSA with h$_{top}$.

| Htop (km) | Hypocenter (km) | Percentage Reduction (%) | |
|---|---|---|---|
| | | Minimum Value | Maximum Value |
| 13 | 22.5 | 43.5 | 84 |
| 23 | 32.5 | 58.7 | 83.3 |
| 33 | 42.5 | 59 | 90 |
| 43 | 52.5 | 61.5 | 93 |

that is at bedrock), PSA increased compared to that of $h_{top}$ 33 km, by 5-10%. This could possibly be due to the higher density contrast of the lowest strata as compared to the top three layers, for similar $V_p/V_s$ ratio. Minimum and maximum percentage reduction in PSA compared to $h_{top}$ 3 km case, across all time periods, are reported in Table (4). For the kind of velocity model considered here, and for shallow focus earthquakes of fixed magnitude, it can be concluded that we are safer at least by a factor of 2 from earthquakes happening 20-40 km deep than the ruptures closer to or reaching the surface.

## 7. Discussion and Conclusion

We have shown by finite element simulation of kinematic earthquake rupture that realistic synthetic earthquake accelerograms can be generated at sufficiently dense distribution of near-field stations for time history analysis of structures. Time history analysis is the most accurate way of assessing the structural response in earthquake engineering field as it considers the entire accelerogram. Response spectrum method of earthquake resistant design considers the spectral accelerations values given by the response spectrum of an earthquake at all the natural frequencies of the structure. As response spectrum already is peak response of a single degree of freedom structure at any time period, combining these maximum according to the modal combination rules in building codes gives a conservative estimate of response of structure for which the performance level can be assessed to be in the operational state or possibility of immediate occupancy or if there is a threat to life safety.

We have quantified such response spectrum of a strike-slip earthquake for the range of possible values of ductility of engineered structures, and certain depths at which typical strike-slip events happen. In case of unavoidable circumstances of engineering construction at locations of active faults, these response spectra allow for quick computation of the upper bound of response of the envisioned structure in that area depending on its orientation with respect to the faulting. This work can further be extended to another type of faultings like normal faults and thrust faults of various dip angles.

In Sikkim region of India, where near vertical faulting can be found, the trends of increase or decrease in spectral acceleration with respect to hypocentral depth can be readily extrapolated from
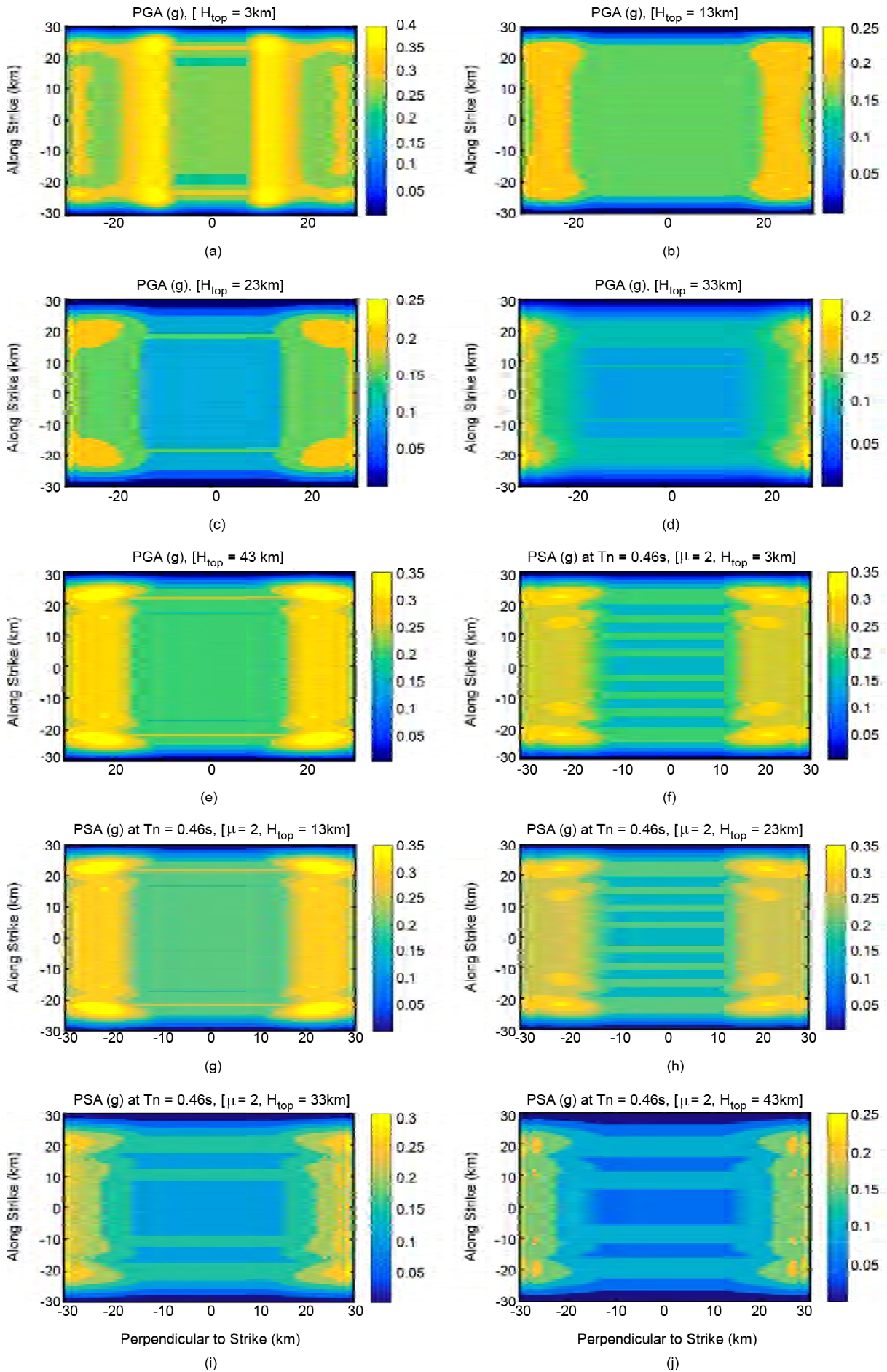
**Figure 14.** Variation of PGA (g), PSA (g) at time period of 0.46 sec and ductility ratio 2 with $h_{top}$.
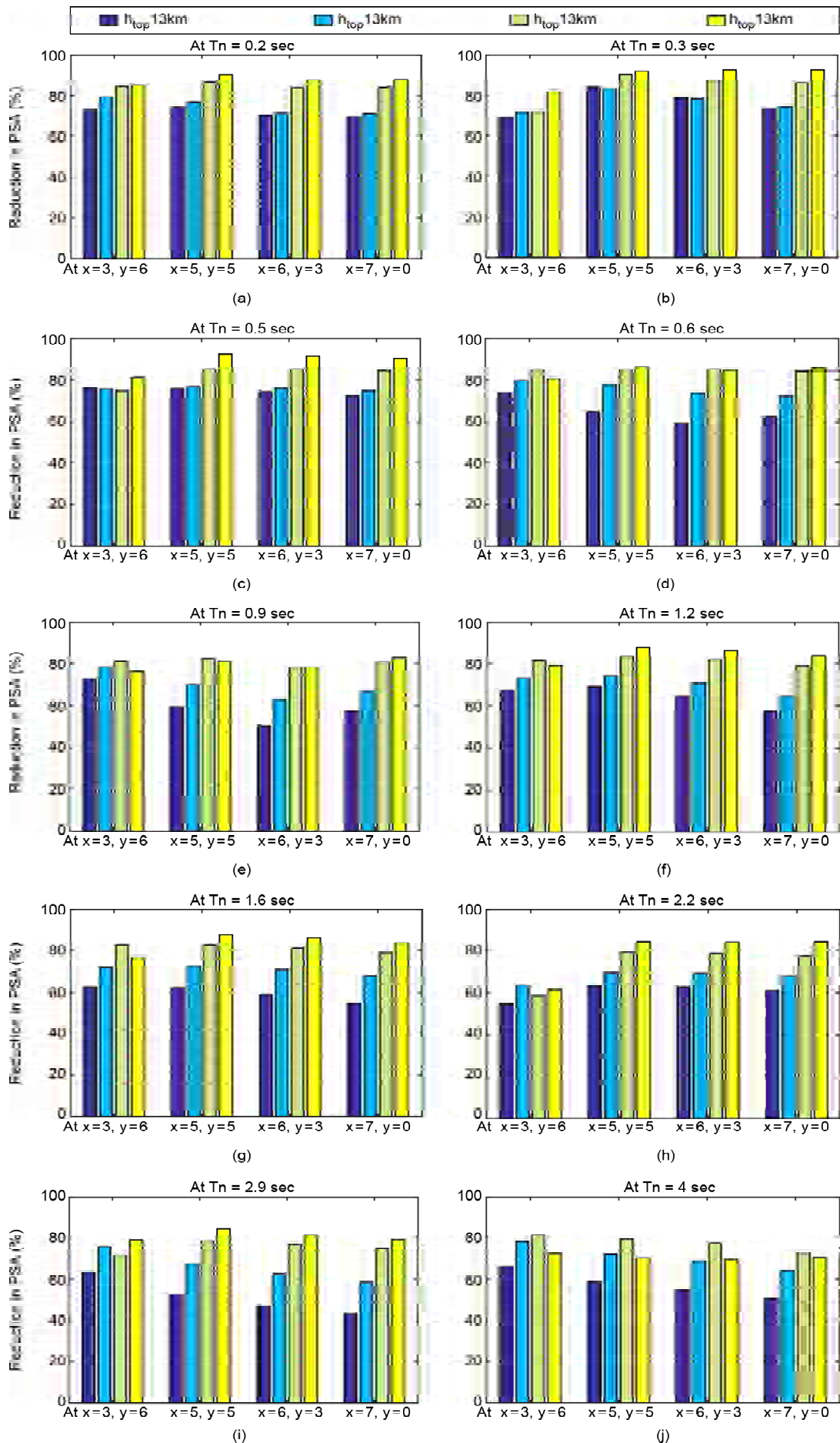
**Figure 15.** Bar diagrams shows percentage reduction in elastic PSA value with $h_{top}$, while $h_{top}$ 3 km is reference case.

the results presented in this work, as the velocity model considered in all the simulations belong to Sikkim region. Care must be exercised while applying results of this work to other vertical strike-slip faulting across the globe as the velocity model perturbations can significantly alter the frequency content of the ground motion.

Scenario-based earthquake simulations are the way forward in getting the plausible values of spatial distribution of ground shaking as a function of time, with respect to a pre-existing structural discontinuity in the earth. The earthquake acceleration can be different at several supports of a multi-span bridge and in such cases to compute a reasonably accurate accelerogram at each of the supports requires detailed modeling of the ground underneath incorporating the large-scale fractures that exist in the earth's crust.

## Acknowledgement

## References

1. Mavroeidis, G.P., Dong, G., and Papageorgiou, A.S. (2004) Near-fault ground motions, and the response of elastic and inelastic single-degree-of-freedom (SDOF) systems. *Earthquake Engineering and Structural Dynamics*, **33**(9), 1023-1049.

2. Campbell, K.W., and Bozorgnia, Y. (2008) NGA ground motion model for the geometric mean horizontal component of PGA, PGV, PGD and 5% damped linear elastic response spectra for periods ranging from 0.01 to 10 s. *Earthquake Spectra*, **24**(1), 139-171.

3. Aagaard, B., Kientz, S., Knepley, M., Strand, L., and Williams, C. (2013) *PyLith User Manual, Version 2.1.0.*, Davis, CA: Computational Infrastructure of Geodynamics.

4. Balay, S., Gropp, W.D., McInnes, L.C., and Smith, B.F. (1997) Efficient management of parallelism in object-oriented numerical software libraries. *Modern Software Tools for Scientific Computing*, 163-202, Birkhauser Boston.

5. Blacker, T.D., Bohnhoff, W.J., and Edwards, T.L. (1994) *CUBIT Mesh Generation Environment.* Volume 1: Users' Manual (No. SAND--94-1100). Sandia National Labs., Albuquerque, NM (United States).

6. Liu, P. and Archuleta, R.J. (2004) A new nonlinear finite fault inversion with three-dimensional Green's functions: Application to the 1989 Loma Prieta, California, earthquake. *Journal of Geophysical Research: Solid Earth*, **109**(B2).

7. Somerville, P.G. (2003) Magnitude scaling of the near fault rupture directivity pulse. *Physics of the Earth and Planetary Interiors*, **137**(1), 201-212.

8. Mai, P.M. and Beroza, G.C. (2000) Source scaling properties from finite-fault-rupture models. *Bulletin of the Seismological Society of America*, **90**(3), 604-615.

9. Mai, P.M. and Beroza, G.C. (2002) A spatial random field model to characterize complexity in earthquake slip. *Journal of Geophysical Research: Solid Earth*, **107**(B11).

10. Andrews, D.J. (1976) Rupture velocity of plane strain shear cracks. *Journal of Geophysical Research*, **81**(32), 5679-5687.

11. Liu, P., Archuleta, R.J., and Hartzell, S.H. (2006) Prediction of broadband ground-motion time histories: Hybrid low/high-frequency method with correlated random source parameters. *Bulletin of the Seismological Society of America*, **96**(6), 2118-2130.

12. Iman, R.L. (2008) *Latin Hypercube Sampling.* John Wiley & Sons, Ltd.

13. Acton, C.E., Priestley, K., Mitra, S., and Gaur, V.K. (2011) Crustal structure of the darjeeling-Sikkim Himalaya and Southern Tibet. *Geophysical Journal International*, **184**(2), 829-852.

14. Paul, H., Mitra, S., Bhattacharya, S.N., and Suresh, G. (2015) Active transverse faulting within under thrust Indian crust beneath the Sikkim Himalaya. *Geophysical Journal International*, **201**(2), 1070-1081.